JOURNAL OF MATERIALS SCIENCE 27 (1992) 5463–5469

Sol–gel prepared Ni–alumina composite materials

Part II *Structure and hot-pressing temperature*

E. BREVAL, C. G. PANTANO*
*Materials Research Laboratory and *Department of Materials Science and Engineering, The Pennsylvania State University, University Park, PA 16802, USA*

The microstructure of sol–gel prepared Ni–alumina ceramic–metal composites containing up to 50% Ni has been studied with X-ray diffraction, the scanning electron microscope and the transmission electron microscope. The influence of processing temperature upon the size distribution of Ni was established. It was found that increasing the total amount of Ni increases only the number of micrometre-size Ni inclusions in the alumina, whereas the hot-pressing temperature determines the size distribution of Ni. When temperatures much higher than the melting temperature of Ni are used, a large number of Ni inclusions of the order of 10 nm can be found mainly within alumina grains; only a few are formed in grain boundaries and in triple points. When a temperature close to the melting point is used, there are fewer nanometre-size Ni inclusions and a larger number of Ni inclusions of the order of ~100 nm to 1 μm. In this case, the large (~100 nm) and small (~10 nm) Ni inclusions are found in grain boundaries and triple points.

1. Introduction

It has been shown [1] that in order to synthetize homogenous and dense Ni–alumina composites with Ni contents up to 50%, it is necessary to hot-press the sol–gel-derived powder precursor at temperatures close to or above the melting temperature of Ni; cold pressing and sintering yield porous and dewetted metal composites. In general, it was found that a larger number of micrometre-size Ni inclusions occurred with increasing Ni content. Now, a closer study of how the processing temperature influences the microstructure is considered to be of importance, because the Ni dispersion so critically determines mechanical properties such as the wear resistance of the ceramic. The metastability of the sol–gel precursor is undoubtedly of importance in establishing the mechanism through which the final microstructure of the Ni–alumina composite is developed. So too, the hot-pressing temperature, relative to the melting point of Ni (1453 °C), is an issue.

The purpose of this paper is to report the study of Ni–alumina composites, especially the distribution of metal and possible grain boundary phases, and to correlate the findings with the amount of Ni in the ceramic composite and with the hot-pressing temperature.

One of the main concerns is the distribution of metal; that is, whether it appears as inclusions or along grain boundaries as crystalline or amorphous material. The detection of nanometre-scale grain boundary material has been reviewed by Clarke [2] who describes three TEM methods: the high-resolution lattice image method, the high-resolution bright-field method, and the high-resolution dark-field method. A thorough description of the latter is discussed by Simpson *et al.* [3] who explain how to distinguish between a true amorphous grain boundary phase and a contaminated surface groove in the grain boundary, filled with amorphous waste products from the ion-beam thinner. This method leaves little possibility for error; it is quick and can therefore be carried out repeatedly within a reasonable time; for that reason, it has been adopted in the present study. Also, a single-crystal dark-field or bright-field method has been used to contrast Ni metal against adjacent Al_2O_3 grains. A sintered alumina containing a glassy grain boundary phase [4] is compared with the present findings.

2. Experimental procedure

The synthesis and hot pressing procedures are described in detail in an earlier report [1]; see also Table I giving the densities [1] and hot-press temperatures. The general structures of the specimens studied in the SEM have already been described [1] in terms of micrometre-size Ni inclusions. Since hot isostatic pressing was performed on disc-shaped material of ~ 0.5 cm thickness and with an area of ~ 10 cm^2, there exists the danger of preferred orientation. In order to verify the uniformity of the pressure during the hot pressing, X-ray diffraction was carried out on

0022–2461 © *1992 Chapman & Hall*

the largest surface, and the intensities from important crystallographic planes in the phases present in the composite were measured.

Each specimen was then cut to discs of 3 mm diameter and ~ 100 μm thickness. One side was pol-

TABLE I Ni–Alumina ceramic composites with indication of density, hot-pressing temperature and ease of grinding/polishing

Ni (wt %)	Density (% of theoretical)	Hot-pressing temperature (°C)	Grindability/ polishibility
0[a]	94	–	–
10	97	1425	Easy
15	90	1854	Medium
20	89	1780	Medium
30	84	1854	Very difficult
50	74	1650	Difficult
50	–	1460	Medium

[a] From Aghajanian *et al.* [4].

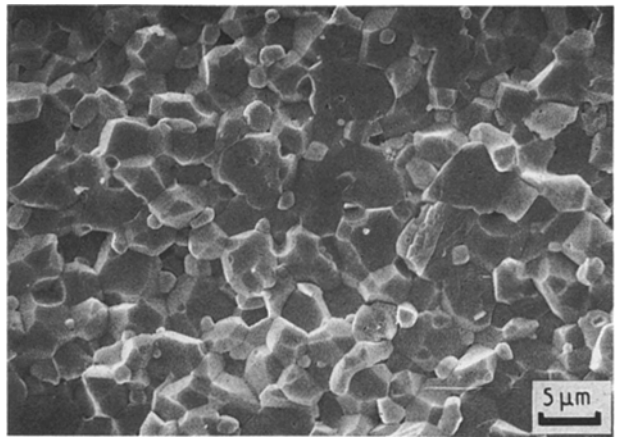

Figure 1 SEM image of fractured surface of an Ni–alumina composite with 15% Ni hot-pressed at a high temperature. The alumina grain size of ~ 5 μm is typical for both low and high temperatures.

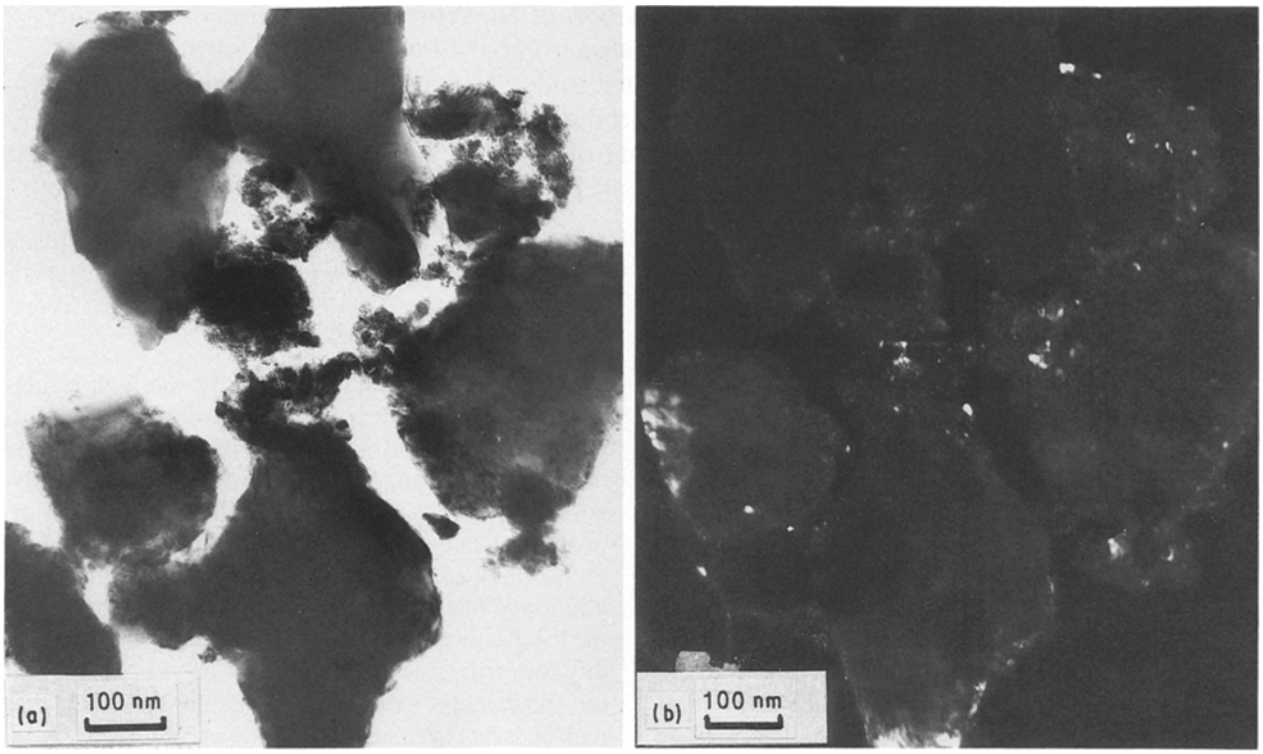

Figure 2 TEM (a) bright- and (b) dark-field imaging of ground nickel–alumina powder used for hot-pressing. Some of the Ni powder is contrasted, showing an extremely good dispersion of Ni powder among the much larger transition alumina grains.

TABLE II XRD intensities of the largest surface of hot-pressed specimens: intensities of selected hkl from Al_2O_3 in ceramic composites

Material	Composition (% Ni)	HP temperature (°C)	Intensity				
			Reference peak	$\parallel Al_2O_3\langle 001\rangle$ $l = 0$		Almost $\perp Al_2O_3\langle 001\rangle$ $l \gg h, l \gg k$	
			$hkl = 113$	$hkl = 110$	$hkl = 030$	$hkl = 006$	$hkl = 018$
Randomly oriented Al_2O_3 Ceramic composite	–	–	100	40	50	< 1	8
	10	1425	100	30	34	2	15
	15	1854	100	40	41	1	24
	20	1780	100	34	40	< 1	9
	30	1854	100	28	33	< 1	12
	50	1650	100	34	46	2	8
	50	1460	100	33	40	1	10

TABLE III XRD intensities of the largest surface of hot-pressed specimens: intensities of selected hkl from Ni in ceramic composites

Material	Composition (% Ni)	HP temperature (°C)	Intensity	
			$hkl = 111$	$hkl = 200$
Randomly oriented Ni	–	–	100	42
Ceramic composite	10	1425	100	37
	15	1854	100	47
	20	1780	100	49
	30	1854	100	38
	50	1560	100	39
	50	1460	100	41

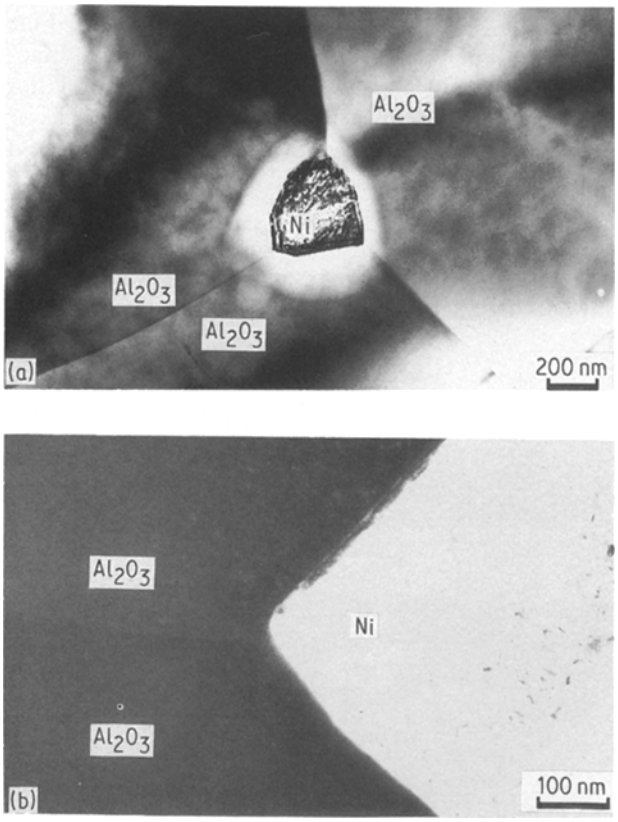

Figure 3 TEM (a) bright-field and (b) dark-field imaging of micrometre-size Ni particle typical for all Ni concentrations and both low and high pressing temperatures. Note the metal grain which does not continue in between two alumina grains.

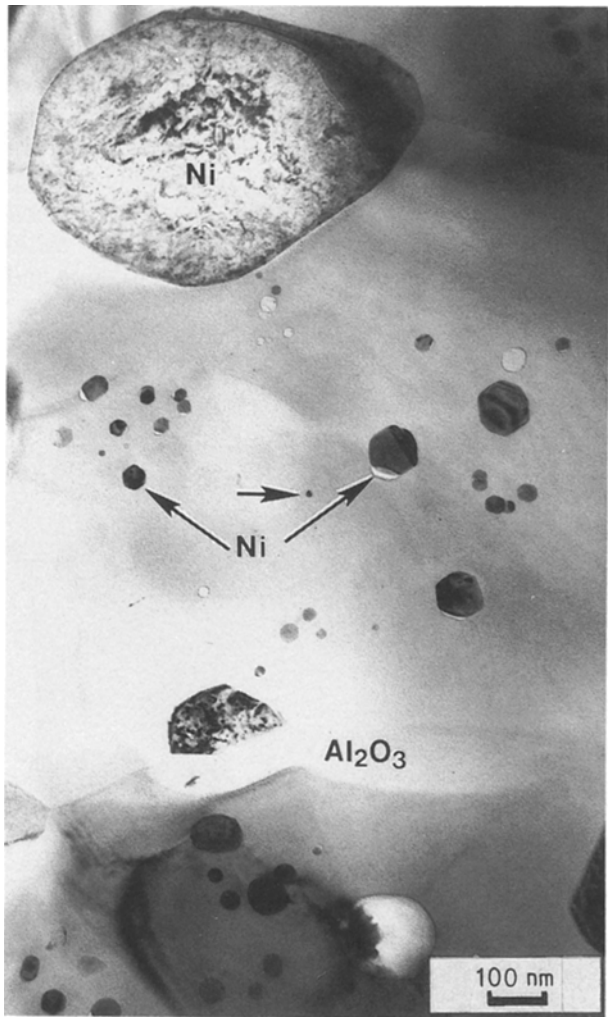

Figure 4 TEM bright-field imaging of nanometre-size Ni grains inside an alumina grain. The example shown is typical for all Ni concentrations and both low and high temperatures of hot pressing, though there are generally more small nanometre-size grains in high-temperature materials.

ished down to a 1 μm finish with diamond paste. The rough side was dimpled and polished to a central thickness of ~ 2 μm. The ease of grinding and polishing was determined qualitatively and is denoted in Table I using the adjectives very difficult, difficult, medium, and easy. The specimens were ion-beam thinned at angles from 20° down to ~ 8° with a gun voltage of 3 to 4 kV, a gun current of 0.5 to 0.7 μA and a specimen current of 3 μA. The structure was then studied in a 120 kV Philips EM 420 TEM fitted with Link energy-dispersive X-ray spectroscopy (EDS). A sintered Al_2O_3 material studied earlier [4] was compared with the ceramic composites. Also, the powder precursor used for hot-pressing was studied in the TEM.

3. Results

Fig. 1 shows an SEM image of a fractured surface of an Ni–alumina specimen with a relatively low content of Ni (15%) hot-pressed at a high temperature (1854 °C). This appearance, showing grains of ~ 5 μm size, is typical for both high- and low-temperature materials. The low Ni content material was chosen because the alumina grains are better imaged than when the material contains a large amount of Ni.

Fig. 2 shows TEM micrographs of the powder used for hot pressing. The bright-field image shows the general particle distribution. The dark-field image contrasts some of the Ni and shows an excellent dispersion of the nanometre-size Ni particles among the much larger transition alumina grains.

Tables II and III give the background-stripped intensities from the X-ray diffraction experiments which show peaks from Al_2O_3 and Ni. The standard deviations are between 10% on larger peaks ($I = 25$ to 50) and $\sim 20\%$ on smaller peaks ($I = 2$ to 25). Table II shows that the orientation of Al_2O_3 in all the composite ceramics is close to a random orientation, which is also shown in the table for comparison. However, there is a tendency for the c-axis of Al_2O_3 ($\langle 0\,0\,0\,1 \rangle$) to be parallel to the normal of the specimen disc. The orientation of Ni in all the composites shown in Table III is very close to random (also shown).

The qualitative ease of grinding and polishing indicates generally that low temperatures and a high metal content give composites that are easy to grind and polish, whereas high temperatures and a low metal content give composites that are difficult to grind and polish.

The TEM micrographs in Figs 3 to 9 show clearly how Ni inclusions of micrometre and nanometre size are formed in a continuous Al_2O_3 phase in all specimens. General features (Figs 3 and 4), typical for both low and high temperatures, are the Ni inclusions in triple points and nanometre-size Ni inclusions found inside Al_2O_3 grains. At low temperatures, three features are characteristic: elongated Ni inclusions of micrometre size, the tendency for some Ni grains to continue partly out into the grain boundary between Al_2O_3 grains, and the position of many Ni inclusions on Al_2O_3–Al_2O_3 grain boundaries and triple points rather than inside the Al_2O_3 grains (see Figs 5 to 7). The features for high-temperature composites are shown in Figs 8 and 9 where the presence of some large (~ 100 nm to 1 μm) and many small (nanometre-size) Ni inclusions can be observed. The latter can appear either on grain boundaries/triple points or inside alumina grains. Both micrometre-size and nanometre-size Ni inclusions often contain (1 1 1) twins.

No amorphous grain boundary phases were found in the sol–gel prepared specimens prepared at either low or high temperatures. For comparison, Fig. 10

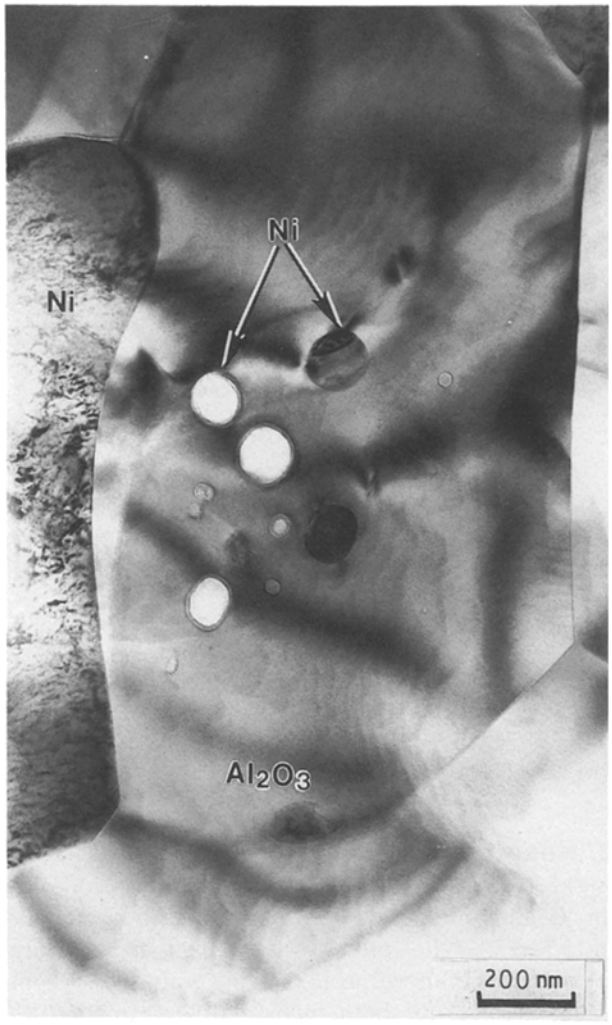

Figure 5 TEM bright-field imaging of micrometre-size Ni particles often found in all low-temperature materials. The larger metal inclusions are often elongated rather than spherical.

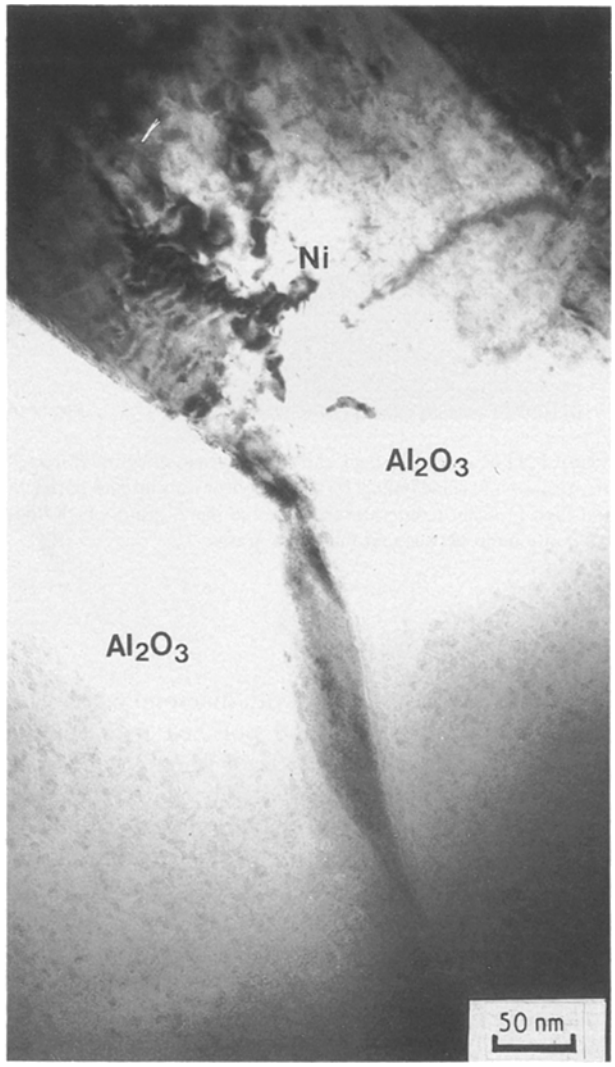

Figure 6 TEM bright-field imaging of 50 to 500 nm Ni particles typical for low-temperature material. The metal has sometimes a tendency to continue partly in between two alumina grains.

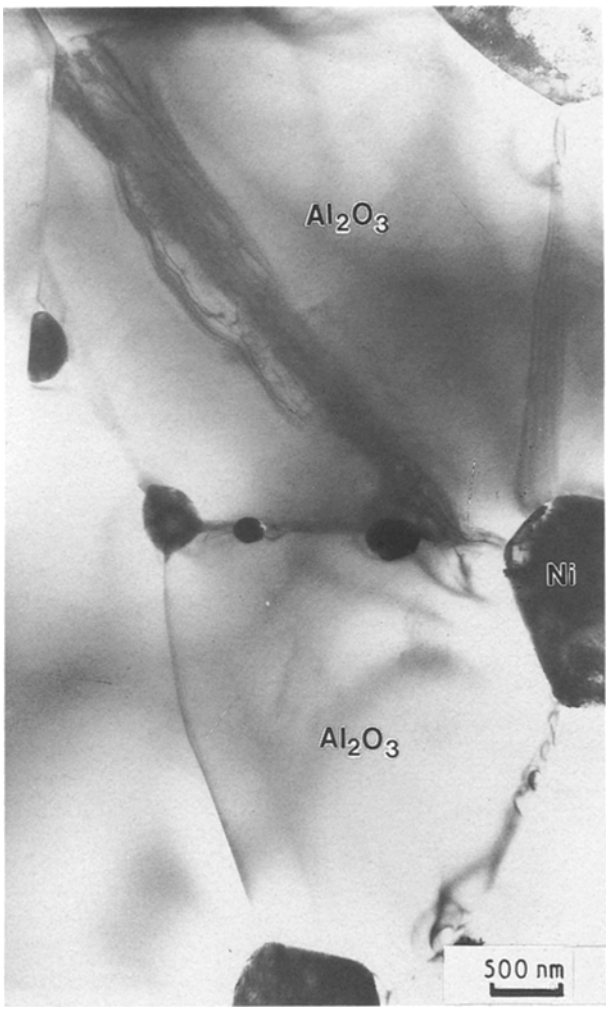

Figure 7 TEM bright-field imaging of several Ni particles in the alumina matrix typical for low-temperature materials. The metal particles are related to Al_2O_3–Al_2O_3 grain boundaries and are often positioned at triple points.

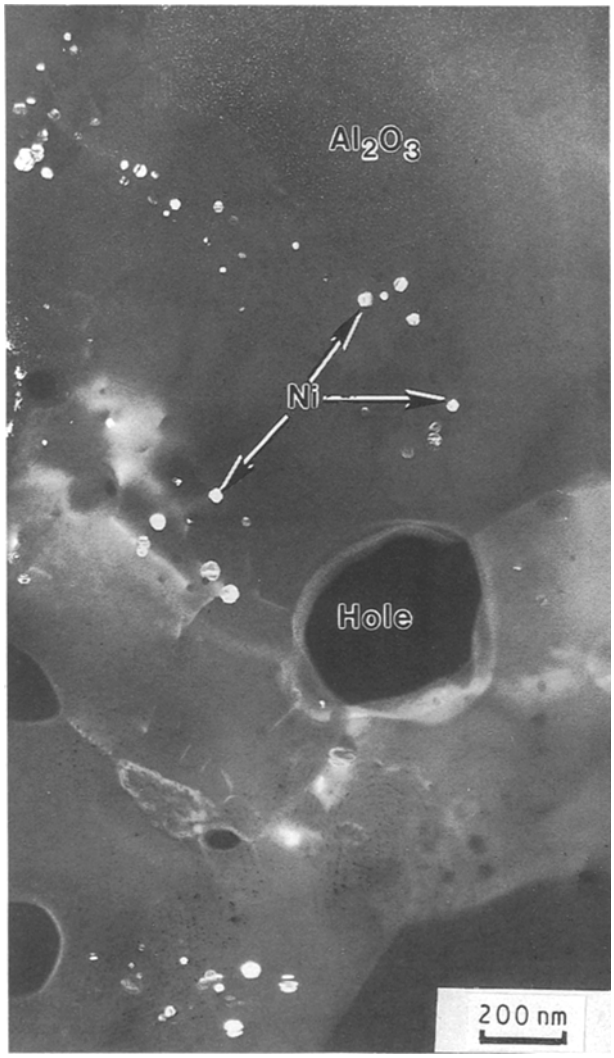

Figure 8 TEM bright-field imaging of Ni particles in alumina typical for high-temperature materials. There are many nanometre-size Ni particles inside the alumina grains.

shows a dark-field image of a typical glassy grain boundary phase in a sintered alumina described earlier [4].

Fig. 11 is a sketch showing the structure of the powder precursor and the Ni–alumina hot-pressed at low temperatures and high temperatures, respectively.

3. Discussion

The appearance of many small metal inclusions in the alumina, especially the intragranular Ni, is clearly correlated with the observed difficulty of grinding and polishing. Nevertheless, the amount of Ni metal has importance because the ceramics with the larger amounts of metal were more easy to grind. These qualitative observations are considered to be related to the wear resistance of these materials.

The solubility of Ni in Al_2O_3 is reported to be negligible [5, 6]. It has been reported that, at $\sim 1450\,^{\circ}C$ and 50 to 700 MPa, a reaction zone of Ni_2Al_3 will appear between Ni and Al_2O_3 [7]; however, this was not observed in the present investigation (1425 to 1800 °C and 17 MPa). It is not likely that the presence of Ni inclusions within individual alumina grains is due to solubility or precipitation effects [8].

More likely, the small nanometre-scale Ni inclusions within the Al_2O_3 grains were trapped during the final stages of the α-Al_2O_3 transformation, or during exaggerated grain growth. There is evidence to support both of these ideas. Pugar and Morgan [9] found a very fine-grained intragranular ZrO_2 phase in sol–gel-derived Al_2O_3–10% ZrO_2. They concluded that the ZrO_2 was engulfed by the transforming transitional alumina colonies to become encapsulated in the densified α-Al_2O_3 grains. Similarly, there are many documented examples [10] of exaggerated grain growth in Al_2O_3 grains. Both of these effects are enhanced at elevated temperatures.

Fig. 11 is a schematic description of the microstructural evolution that is believed to occur in the Ni–Al_2O_3 ceramics. The precursor powder was obtained by heating an Ni-doped behmite gel to 1000 °C in hydrogen to create an ultrafine-grained dispersion of Ni particles within transitional alumina. At low hot-pressing temperatures, the rate of transformation/densification is slow, and so the Ni phase coarsens and/or sweats from the transitional alumina. In this way the grain growth is limited, and most of the Ni phase is *inter*granular within the final densified ceramic. At the higher hot-pressing temperatures, the

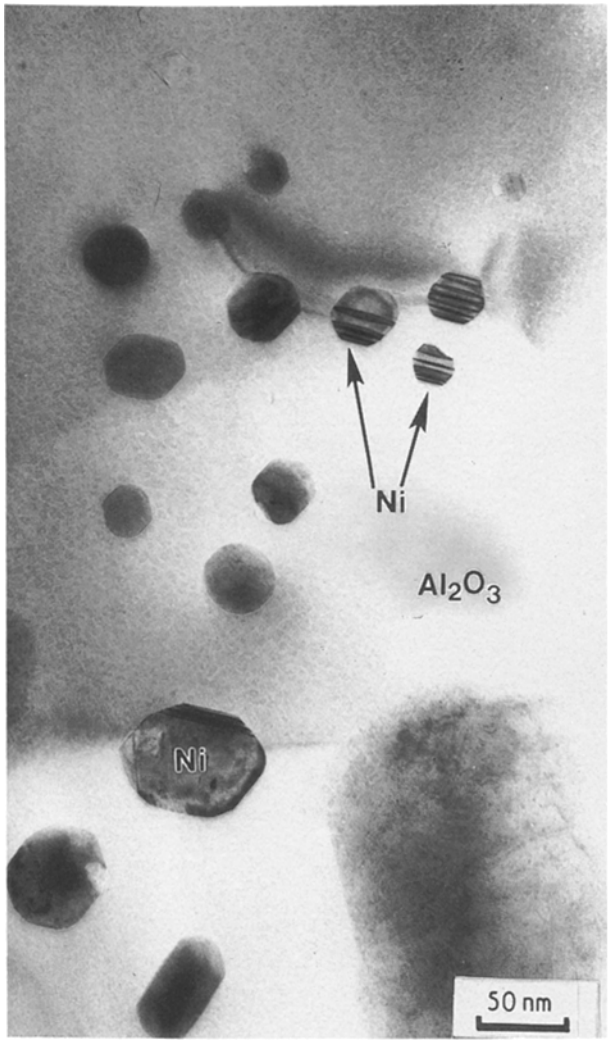

Figure 9 TEM bright-field imaging of nanometre-size Ni particles in alumina typical for high-temperature materials. Sometimes the small Ni particles in the alumina are connected via low-angle Al_2O_3–Al_2O_3 grain boundaries.

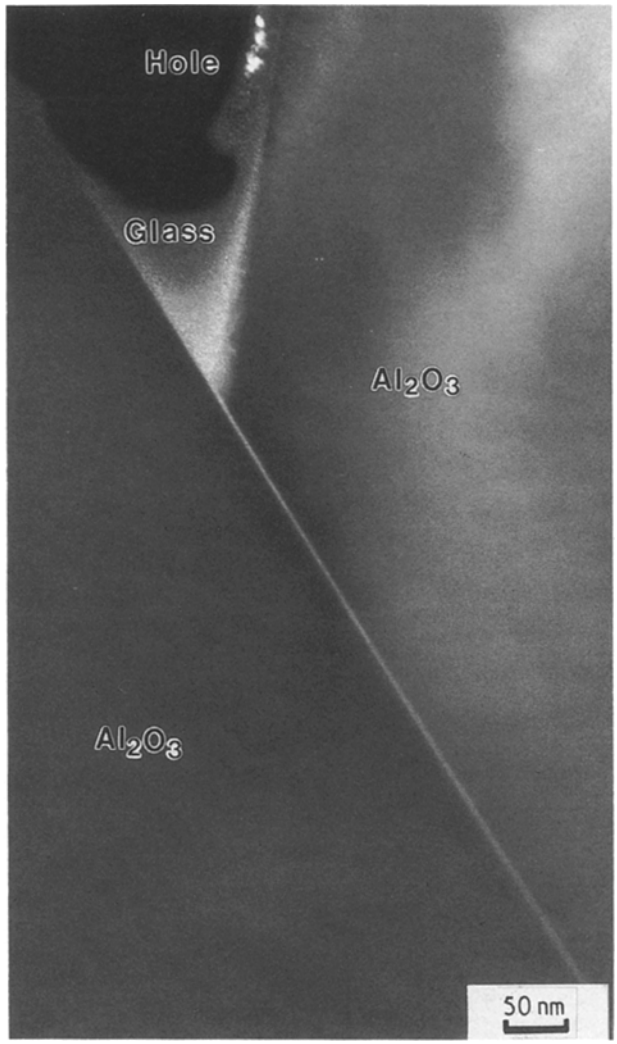

Figure 10 TEM dark-field imaging of amorphous grain-boundary phase in sintered alumina situated in a triple point and continuing in between two Al_2O_3 grains.

transformation/densification rates are high. Thus, the ultrafine-grained Ni phase may become trapped within transitional alumina colonies, and ultimately within the dense α-Al_2O_3 grains. Furthermore, the grain boundary migration rate will be enhanced due to the higher temperature and due to the reduced Ni content in the boundaries; thus, grain boundaries may break away from the Ni. Altogether, this leads to a structure wherein the original Ni particles form an *intra*granular phase during the transformation and/or grain growth. The observed presence of low-angle grain boundaries within the large grains of α-Al_2O_3 (which contain the small nanometre-scale Ni inclusions) is more consistent with the importance of the α-Al_2O_3 transformation, than the exaggerated grain growth, in determining the final microstructure.

4. Conclusions

Sol–gel prepared Ni–alumina ceramic–metal composites containing up to 50% Ni consist of Ni inclusions with a continous polycrystalline Al_2O_3 microstructure. The Ni inclusions are randomly oriented, and are found to be both *inter*granular and

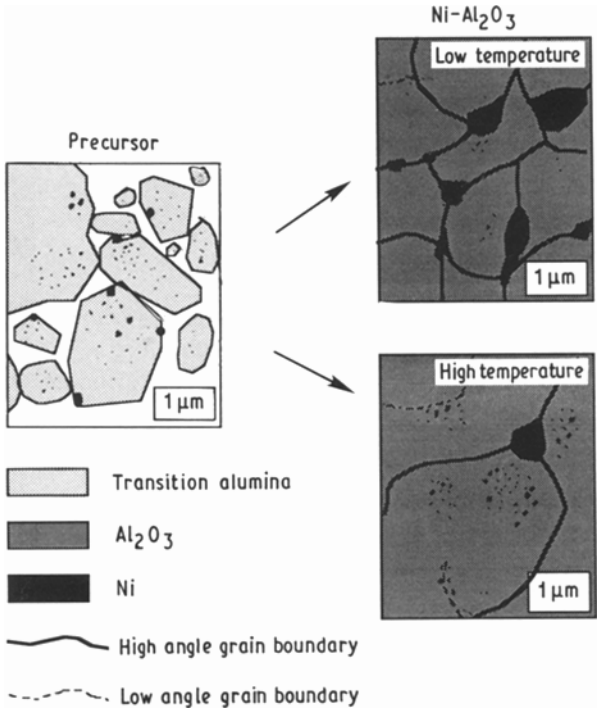

Figure 11 Sketch showing the microstructure of the powder precursor and of the Ni–alumina ceramic hot-pressed at low temperature and high temperature, respectively.

*intra*granular. The microstructural evolution depends primarily upon the hot-pressing temperature. When high temperatures are used, a large number of Ni inclusions of the order of 10 nm can be found, mainly within the individual alumina grains, and only a few are formed in grain boundaries and in triple points. When lower temperatures are used, a larger number of Ni inclusions of the order of $\sim$ 100 nm to 1 μm, and only few nanometre-size intragranular Ni inclusions are found. Continuous grain boundary phases are not present in any case. The higher hot-pressing temperatures yield microstructures that are more resistant to grinding and polishing and this is clearly due to the presence of the intragranular Ni phase. It is expected that these materials will exhibit good wear resistance.

Acknowledgements

The experimental work was funded by the Center for Advanced Ceramics' Co-op Program at Penn State University and by NSF (DMR-8812824). The authors want to thank Z. Deng for preparation of the specimens and S. Chiou for the X-ray work.

References

1. E. BREVAL, Z. DENG, S. CHIOU and C. G. PANTANO, *J. Mater. Sci.* **27** (1992) 1464.
2. D. R. CLARKE, *Ultramicroscopy* **4** (1979) 33.
3. Y. K. SIMPSON, C. B. CARTER, K. J. MORISSEY, P. ANGELINI and J. BENTLEY, *J. Mater. Sci.* **21** (1986) 2689.
4. M. K. AGHAJANIAN, E. BREVAL, J. S. JENNINGS and N. H. MACMILLAN, *ibid.* **21** (1986) 2819.
5. R. WINZER, *Angewandte Chemie*, **45** (1932) 429.
6. G. GRUBE and K. RATSCH, *Z. Elektrochem.* **45** (1939) 838.
7. I. P. ARSENTYEVA and M. M. RISTIC, in "Sintered Metal–Ceramic Composites", edited by G. S. Upadhyaya (Elsevier Science, Amsterdam, 1984) 181.
8. "Phase Diagrams", Vols. I–V (American Chemical Society, Columbus, OH, 1965–85) pp. 16, 4150.
9. E. A. PUGAR and P. E. D. MORGAN, *J. Amer. Ceram. Soc.* **69** (1986) C-120.
10. W. D. KINGERY, "Introduction to Ceramics" (Wiley, New York, 1976) p. 461.

Received 3 June
and accepted 2 October 1991